

Article

Characteristics and Trends of Ambient Ozone and Nitrogen Oxides at Urban, Suburban, and Rural Sites from 2011 to 2017 in Shenzhen, China

Dian Huang ^{1,2} , Qinglan Li ^{2,*}, Xiaoxue Wang ², Guangxin Li ², Liqun Sun ², Bing He ², Li Zhang ³ and Chunsheng Zhang ³

¹ College of Urban and Environmental Sciences, and Key Laboratory for Earth Surface Processes of the Ministry of Education, Peking University, Beijing 100871, China; huangdian@pku.edu.cn

² Shenzhen Institute of Advanced Technology, CAS Joint Engineering Research Center for Health Big Data Intelligent Analysis Technology, Chinese Academy of Sciences, Shenzhen 518055, China; ql.li@siat.ac.cn (Q.L.); xx.wang@siat.ac.cn (X.W.); ligx@siat.ac.cn (G.L.); lq.sun@siat.ac.cn (L.S.); bing.he@siat.ac.cn (B.H.)

³ Shenzhen Meteorological Bureau, Shenzhen 518040, China; ziluolan_123@163.com (L.Z.); zhangchunsheng@szmb.gov.cn (C.Z.)

* Correspondence: ql.li@siat.ac.cn; Tel.: +86-131-2889-0309

Received: 15 November 2018; Accepted: 26 November 2018; Published: 1 December 2018



Abstract: The emissions of nitrogen oxides (NO_x) decreased under China's air quality control policies. However, concern remains regarding the response of ozone (O₃) in the metropolitan areas. The characteristics and trends of ambient O₃ and NO_x in Shenzhen were investigated during the 2011–2017 period. Both the human population and vegetation are exposed to higher O₃ at suburban and rural sites than at the urban site. The O₃ weekend effect is significant ($p = 0.062$) at the urban site, with O₃ levels 1.19 ppb higher on Sunday than on weekdays. Solar radiation, precipitation, and relative humidity are the most relevant meteorological factors that affect O₃ daily variations. Wind speed is the least relevant factor, but wind direction is related to the presence of high O₃ air concentrations. Both 1-h and 8-h O₃ exhibit an increase, opposite to the trend of NO_x. A slight decline in O₃ occurs in autumn at less urbanized sites. The increase in O₃ is more prevalent and rapid in the winter at more urbanized sites. This can be due to the transport of increased O₃ from northern China, as well as a lowered O₃ titration effect with NO_x reduction. O₃ increases fastest at the urban site, with an estimated rate of 4.3% (95% confidence intervals (CIs): 0.96, 8.25) per year ($p < 0.05$) for 8-h O₃ and 2.5% (95% CIs: −0.46, 6.12) per year ($p > 0.1$) for 1-h O₃, posing greater human health risks to areas with high population density.

Keywords: ozone; nitrogen oxides; urban and rural; meteorological factors; trends; Shenzhen

1. Introduction

China's rapid economic growth and urbanization greatly increased energy consumption and air pollutant emissions since economic reforms in 1978 [1]. Environmental monitoring campaigns carried out in urban centers highlighted O₃ values that are of concern for human health [2,3]. Elevated surface ozone (O₃) is a growing environmental concern in China [1–5]. Serious O₃ episodes are frequent in China's most economically vibrant and densely populated regions, such as the Beijing–Tianjin–Hebei (BTH) area and the Yangtze River Delta (YRD) and Pearl River Delta (PRD) regions [5]. Studies showed substantial detrimental effects of elevated ground-level O₃, including declining forest ecosystem services, crop yield loss, and associated premature deaths [4,6,7].

Tropospheric O₃ is formed by a series of complex nonlinear photochemical reactions between O₃ precursors, namely methane, carbon monoxide, volatile organic compounds (VOCs), and nitrogen oxides (NO_x = NO + NO₂) [8]. Because NO_x is mainly anthropogenic, control of O₃ is usually through NO_x regulation [9]. In China's 12th five-year plan (2011–2015), the goal was set to reduce national NO_x emissions by 10% relative to the 2010 level [10]. Both satellite retrievals and emission inventories show success in reducing NO_x emissions nationwide [11–15]. Compared with other large NO_x emission regions such as BTH and YRD, the decline in NO_x emissions in the PRD region started earlier in 2005 [11,14].

Shenzhen is a major megacity in the PRD region and a twin megalopolis to Hong Kong. Shenzhen was established as China's first Special Economic Zone in 1980 and developed from a small village into a large metropolitan area with a population over 10 million in three decades. Accompanied by rapid economic growth, the air quality in Shenzhen deteriorated [16]. Epidemiologic studies showed significant associations between O₃ levels and increased mortality and respiratory diseases in Shenzhen [17,18]. To tackle air pollution issues, the governments of Guangdong Province and Hong Kong worked closely to reduce emissions of SO₂, NO_x, and VOCs throughout the region [19]. In addition to national and regional environmental control efforts, Shenzhen also implements energy reforms for public transportation and private motor vehicles. It is the world's first city that electrified 100% of public buses and will electrify all taxis by the end of 2020 [20]. The decline in NO_x emissions is fastest in Shenzhen compared with other megacities like Shanghai, Beijing, and Guangzhou [11].

NO_x regulation showed effectiveness in reducing peak O₃ levels over the long term and elevated mean O₃ levels at the same time [21–24]. However, due to the nonlinear relationship between NO_x and O₃, NO_x control might worsen the O₃ problems in urban areas in the short term [19,25]. This is mainly caused by the lessened titration effect of NO in urban areas, where the O₃ photochemical chemistry is mainly VOC-sensitive [21–24]. Simulation results showed that peak O₃ levels could be effectively reduced in the PRD region when cutting down NO_x and VOC emissions [15,19,25]. Recent observations showed that annual mean O₃ levels were increasing at both urban and suburban sites in the PRD region [24]. However, the changes in peak O₃, which is closely related to human health, are rarely shown by observation data.

Apart from emissions of O₃ precursors, meteorological factors are also important in affecting O₃ levels both directly and indirectly. Meteorological factors can directly impact the formation of O₃ because the reactions are sensitive to the changes in sunlight and temperature [5,26,27]. Meteorological factors such as wind speed, surface pressure, and precipitation also impact the accumulation, dilution, and deposition of O₃ [5,27–29]. The prevailing wind direction that changes with the season is closely related to air pollutant transport from near and distant areas [5,27,28]. Actually, the relationship between air pollutants and meteorological factors varies greatly by geographical location and season [5]. The investigation of the relationship between O₃ and meteorological parameters in Shenzhen will help understand the pollution situation in the PRD region, as well the large cities that are close to Shenzhen, namely Hong Kong and Macau.

The characteristics of O₃ at urban, suburban, and rural sites depend on the O₃ photochemical sensitivity of the region. One previous study reported higher 1-h and 8-h O₃ in central areas of Shenzhen, which is uncommon for most large cities [17]. Higher urban O₃ is a possible pattern for some cities, e.g., Atlanta and Houston, where large sources of VOCs originate from biological and anthropogenic emissions [30,31]. For most populous areas in the PRD region, the photochemical regime was indicated as VOC-sensitive, with a mixed or transitional regime in Shenzhen [32]. Studying the spatial O₃ pattern between urban and rural areas will help determine the controlling precursors related to the O₃ production rate, which is critical for O₃ control and management.

The comprehensive monitoring of O₃ and NO_x by the Shenzhen Meteorological Bureau was carried out at four air monitoring sites, starting in 2010. This is three years earlier than the introduction of CAAQS GB 3095–2012 in Shenzhen in 2013, allowing us to analyze the spatial and interannual variations of air pollutants. In this study, we investigate the characteristics and trends of O₃ at urban,

suburban, and rural sites of Shenzhen based on seven years of observations of O_3 and NO_x from 2011 to 2017. Our objectives were to (1) assess and compare O_3 risks to human and plants at urban, suburban, and rural sites; (2) investigate weekly and monthly O_3 and NO_x variations and their influences; and (3) evaluate O_3 and NO_x trends during the 2011–2017 period.

2. Data and Methods

2.1. Sites

Shenzhen is the second largest populated city in the PRD region and located to the north of Hong Kong. Figure 1 illustrates the location of Shenzhen and four O_3 monitoring stations, Zhuzilin (ZZL), Shiyan (SY), Longgang (LG), and Xichong (XC). The urban site ZZL ($22^{\circ}32'28.94''N$, $114^{\circ}0'17.15''E$, 63 m elevation) is in the Futian District and had a population density of $19091/km^2$ in 2016 [33]. It is within the original boundary of the Special Economic Zone (former SEZ), which is one of Shenzhen's earliest developed regions, with well-established high-density commercial and residential areas. Two suburban sites, SY ($22^{\circ}39'13''N$, $113^{\circ}53'37''E$, 51 m) and LG ($22^{\circ}43'27''N$, $114^{\circ}14'32''E$, 90 m) were in the Bao'an and Longgang districts with moderate population densities of $7607/km^2$ and $5522/km^2$, respectively. Rural coastal site XC ($22^{\circ}28'52.95''N$, $114^{\circ}31'35.16''E$, 19 m) is on the Dapeng Peninsula, far from the downtown area. It had a population density of $477/km^2$ and is greatly impacted by the land–sea breeze circulation. In addition to O_3 , NO_x concentrations are monitored at ZZL and XC. Hourly O_3 and NO_x data were analyzed for the 2011 to 2017 period. Meteorological data at SY (solar radiation, wind speed, air temperature, and precipitation, relative humidity, and surface air pressure) from 2014 to 2017 were provided by the Shenzhen Meteorological Bureau.

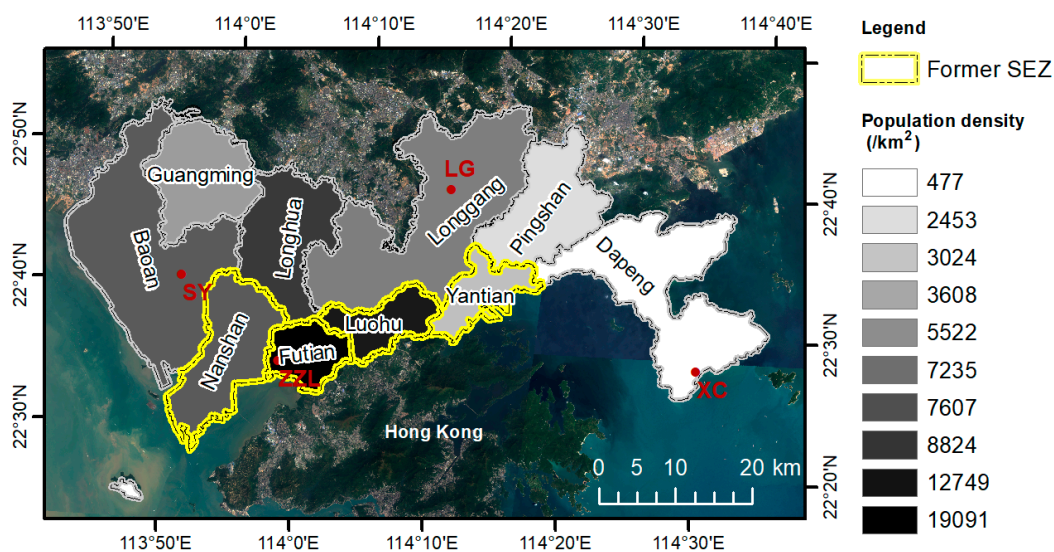


Figure 1. Location of ozone (O_3) monitoring sites at the urban site Zhuzilin (ZZL), suburban sites Shiyan (SY) and Longgang (LG), and the rural coastal site Xichong (XC) in Shenzhen. ZZL and XC also monitor nitrogen oxides (NO_x) concentrations. SY also monitors meteorological parameters.

2.2. Measurement of Air Pollutants

Commercial trace gas instruments (i-Series, Thermo Environmental Instruments Inc., Waltham, MA, USA) were used to continuously measure concentrations of O_3 (Model 49i) and $NO/NO_2/NO_x$ (Model 42i). The O_3 analyzer uses ultraviolet (UV) photometry to detect the absorption of UV radiation from O_3 molecules at a wavelength of 254 nm via the Beer–Lambert law. The working principle of the NO_x analyzer is that NO and O_3 react to produce characteristic luminescence, and its intensity is linearly proportional to the NO concentration (www.thermoscientific.com). Both instruments output ppb by default.

To ensure instrumental accuracy, quality assurance/quality control procedures were applied in strict accordance with the national standard. Automatic zero/span checks of gas analyzers were performed once per day. Manual checks were done bi-weekly, and multipoint calibrations were done after equipment maintenance or at least every six months. The coefficient of determination (R^2) of the linear equation derived by multipoint calibration had to exceed 0.999 for the calibration to be accepted. Calibrations of Model 49i were performed using a portable O_3 transfer standard (Sabio Environmental Model 2030) over the entire study period. The Model 42i was calibrated using a dynamic gas calibrator (Model 146) and a zero air supplier (Model 111). More detailed descriptions of the installation and maintenance procedures are given in the Chinese atmospheric composition monitoring service specification [34].

The validity data rates for O_3 and NO_x at each monitoring site in each year from 2011 to 2017 are listed in Table 1. Except for a large amount of data missing from the LG monitoring station in 2011, the data coverage of all other monitoring stations generally exceeded 70% per year. LG's data missing in 2011 was due to data monitoring delays by external factors at the initial operational stage. Data release did not begin until the end of July.

Table 1. Validity data rates for ozone (O_3) and nitrogen oxides (NO_x) at each monitoring site in each year from 2011 to 2017 (%). ZZL—Zhuzilin; SY—Shiyan; LG—Longgang; XC—Xichong.

Year	ZZL/ O_3	SY/ O_3	LG/ O_3	XC/ O_3	ZZL/ NO_x	XC/ NO_x
2011	94	89	29	90	95	86
2012	100	98	97	99	100	99
2013	98	96	96	96	98	96
2014	99	98	98	97	99	97
2015	99	82	89	89	98	89
2016	87	70	89	90	87	90
2017	94	92	82	88	94	89

2.3. Methods

The Kolmogorov-Smirnov test, histogram, and quantile-quantile (Q-Q) charts were used to verify the normality of air pollutant recording. The results show that both O_3 and NO_x data were not normally distributed. Therefore, most of our analyses were based on nonparametric methods. Data for each station were summarized as annual, seasonal, monthly, daily, and 8-h mean concentrations. The O_3 index AOT40, which is commonly used to assess forest and ecosystem health protection, was calculated as the sum of daylight (8:00 a.m. to 8:00 p.m.) O_3 over the threshold of 40 ppb. Due to the long growing season in southern China (280–320 days), AOT40 was calculated from April to September, which is the season of main vegetation activity [35]. Because AOT40 is a sum and therefore, sensitive to missing data, values for sites with at least 75% of data available were used to ensure the completeness of the measurement series, and the index was corrected with the following equation (1):

$$AOT40 = AOT40_{measured} \times \frac{N_{total}}{N_{avail}}, \quad (1)$$

where $AOT40_{measured}$ was calculated from the available hourly O_3 data, and N_{total}/N_{avail} is the ratio of the total number of hours (the number of days \times 12) divided by total possible hours.

The meteorological parameters were analyzed on a daily basis. Total solar radiation was calculated as the sum of direct and scattered radiation between 7:00 a.m. and 6:00 p.m., the normal daytime hours of local time. Hourly rainfall data were calculated as daily total precipitation. Because daily values contained numerous zeroes, precipitation data were summed on a monthly basis to show the monthly variations in precipitation. All the sum data were also corrected using Equation (1).

To minimize the O_3 variations caused by different amount of O_3 precursor emissions, the relationship between air pollutants and meteorological factors was also analyzed in each season

using Spearman's rank correlation [36]. March, April, and May are considered spring. June, July, and August are considered summer, while September, October, and November are considered autumn. December, January, and February are considered winter. Statistical comparison was performed using the nonparametric Wilcoxon rank-sum test, which is robust for non-normality and the presence of serial correlation [37].

Conditional probability functions (CPF) were also used to plot the percentile wind pollution rose figure [38]. This method is very useful for showing which wind directions are dominated by high concentrations, and gives the probability. In this study, we used percentile values greater than the 90th percentile to represent all the high values. The CPF is calculated as follows:

$$\text{CPF} = \frac{m_{\theta}}{n_{\theta}}, \quad (2)$$

where m_{θ} is the number of samples in the wind θ with mixing ratios greater than some "high" concentration, and n_{θ} is the total number of samples in the same wind sector. This analysis was performed using the R package "openair" [38].

The Theil-Sen (T-S) estimator [39] was used to determine the magnitude and direction of the trend for a given period (i.e., annual and seasonal). This method was chosen because it does not require assumptions about the functional form or statistical distribution of the data and is resistant to outliers. This analysis was also performed using the R package "openair" [38]. Slope estimates as a percentage of change per year were chosen for comparing sites with different levels of air pollutant. The trend T is calculated as follows:

$$T [\%.yr^{-1}] = 100 \left(\frac{C_{end}}{C_{start}} - 1 \right) / N_{years}, \quad (3)$$

where C_{end} and C_{start} are the mean concentrations for the end and start dates, respectively. N_{years} is the number of years. R software was used to perform all statistical analyses and plot the figures [40,41].

3. Results

3.1. Comparison of O_3 and NO_x at urban, suburban and rural sites

Table 2 summarizes a statistical comparison of O_3 and NO_x at urban, suburban, and rural sites from 2011 to 2017. Annual mean O_3 , maximum daily 8-h O_3 , maximum 1-h O_3 , and AOT40 were generally lower at the urban site and higher at the rural site. The suburban sites had intermediate values. Annual mean O_3 , maximum daily 8-h O_3 , maximum daily 1-h O_3 , and cumulative AOT40 at the rural coastal site were 88%, 54%, 32%, and 67% higher, respectively, than those at the urban site. There is no significant difference in the annual mean O_3 between the urban site ZZL and the suburban site SY ($p > 0.05$). The annual mean NO_x levels were significantly higher at the urban site than at the rural coastal site ($p < 0.05$). The median level differences reached as high as 22 ppb (see Table 2).

The AOT40 value from April to September is commonly used by the European Union to guide O_3 control for forest protection [6]. Since there is currently no vegetation standard in China, this method is often used to assess the risk of O_3 pollution to plants [5,7]. Our results show AOT40 was highest at the rural site with a median value of 19.4 ppm·h and lowest at the urban site with a median value of 11.6 ppm·h (Table 2). The AOT40 values in Shenzhen are about 1–3 times higher than the critical values for forest protection (5 ppm·h) based on an estimated production loss of 5% [6].

The latest Chinese O_3 standard (GB 3095-2012) defines two classes for human health protection from O_3 pollution. Class 1 is more stringent and is mainly aimed at remote areas, with critical values of 100 $\mu\text{g}/\text{m}^3$ (~47 ppb, 8-h O_3) and 160 $\mu\text{g}/\text{m}^3$ (~75 ppb, 1-h O_3). Class 2 is mainly targeted at urban/industrial and surrounding rural areas, with critical values of 160 $\mu\text{g}/\text{m}^3$ (~75 ppb, 8-h O_3) and 200 $\mu\text{g}/\text{m}^3$ (~93 ppb, 1-h O_3). The thresholds of Class 1 are comparable with the World Health Organization (WHO) O_3 guidelines, so it can better guide human health protection [42]. Shenzhen,

Hong Kong, and other cities in the PRD region apply to Class 2 standards, but the exceedance rate of Class 1 was also calculated for a more comprehensive evaluation of O₃ impacts in this area.

Table 2. Statistical comparison of NO_x and O₃ at urban, suburban, and rural sites from 2011 to 2017.

Index	U (ZZL)	S (SY)	S (LG)	R (XC)
Annual mean O ₃ (ppb)	23.3 ^a	22.8 ^a	26.4 ^b	43.8 ^c
Daily maximum 8-h average O ₃ (ppb)	33.2 ^a	35.7 ^b	39.2 ^c	51.0 ^d
Daily maximum 1-h O ₃ (ppb)	42.9 ^a	47.3 ^b	49.1 ^b	56.7 ^c
AOT40 (ppm·h)	11.6 ^a	15.5 ^b	13.7 ^a	19.4 ^b
Annual mean NO _x (ppb)	29.1 ^a	-	-	7.1 ^b

Note: U, S, and R indicate urban, suburban, and rural, respectively. Values inside the box represent medians. Different lowercase letters within the same row indicate statistical difference at $p < 0.05$ according to the Wilcoxon rank-sum test. Values with same superscript letters within the same row indicate no significant difference between sites.

Table 3 shows the average percentage of days that exceeded the national ambient O₃ standards. The results show a relatively small exceedance rate (7–16%) of the national Class 2 standards of 1-h and 8-h O₃. The exceedance rate of 8-h O₃ was highest at the rural site and lowest at the urban site. By contrast, there was a much larger exceedance rate (16–59%) of the national Class 1 standards of 1-h and 8-h O₃. The national Class 1 8-h threshold has the same limit as the WHO O₃ guideline, and indicated that about 28% (103 days) of the year had alarm levels that could have adverse impacts on human health at ZZL. The average numbers of over-limit days in a year were 124 days (34%) at SY, 139 days (38%) at LG, and 215 days (59%) at XC (see Table 3).

Table 3. Average exceedance rate over national ambient O₃ standards (GB 3095-2012) at urban, suburban, and rural sites for the 2011 to 2017 period.

Grade	Type	Limit (µg/m ³)	U (ZZL)	S (SY)	S (LG)	R (XC)
Class 1	1-h	160	16%	23%	20%	24%
	8-h	100 [#]	28%	34%	38%	59%
Class 2	1-h	200	9%	13%	8%	8%
	8-h	160	7%	10%	9%	16%

Both regulatory levels are used for a more comprehensive evaluation of O₃ impacts. [#] World Health Organization (WHO) O₃ standard [42].

3.2. Weekly and Diurnal Variations of O₃ and NO_x

No statistical difference in air concentrations O₃ was found between weekdays and weekends at any site, except for the NO_x concentration, which was 2.39 ppb lower on the weekend than on weekdays at the ZZL urban site ($p < 0.1$) (Figure 2a,b). By graphical comparison, the weekday–Saturday O₃ difference was found to be much smaller than the weekday–Sunday difference. Comparing weekday and Sunday O₃ levels, O₃ was 1.19 ppb higher on Sunday than on weekdays at the urban site ($p = 0.062$) (Figure 2c). The NO_x concentration on weekdays was 3.87 ppb higher than on Sunday ($p < 0.01$) (Figure 2d). At the rural site of XC, NO_x concentration on Sunday showed an opposite pattern, i.e., 1.41 ppb higher than on weekdays ($p = 0.43$) (Figure 2d).

As illustrated in Figure 3, NO_x at the urban site ZZL shows typical diurnal variations that are affected by the daily routine of human activities. NO_x levels increase from about 20 ppb at 5:00 a.m. to the initial daily peak of 35 ppb at 8:00 a.m. This period is coincident with the time of the morning rush hour. The synchronous decrease of O₃ from 19 ppb to 14 ppb is mainly caused by the titration effect of NO, which is a dominant reaction when sunlight is limited for O₃ production. Then, O₃ increases rapidly and reaches its daily maximum values of 40 ppb at 3:00 p.m. with an average rate of 3.7 ppb/h. This process is very likely to be caused by local photochemical production. The second daily NO_x peak at the urban site is around 9:00 p.m., later than the evening rush hour (5:30–7:30 p.m.). This second

peak is possibly caused by continuous emissions of NO_x from the movement of heavy diesel-powered trucks, which are only allowed to enter the city after 8:00 p.m. on weekdays if they do not have local license plates.

The two suburban sites exhibit a more pronounced diurnal O_3 pattern with larger diurnal range and higher daily O_3 peaks than the urban site. O_3 at SY decreases slightly in the early morning and reaches its minimum at 7:00 a.m. O_3 increases rapidly before reaching its maximum of about 46.7 ppb at 2:00 p.m. The average increasing rate is 5.1 ppb/h, which is the highest compared with the other three sites. Similarly, O_3 at LG also decreases slightly in the early morning before reaching its maximum of 45.7 ppb at 2:00 p.m. The average increasing rate is about 4.4 ppb/h at LG, which is also higher than that at the urban site. The diurnal O_3 pattern is slightly different at XC. XC has much higher nighttime O_3 levels and a much lower diurnal range of about 16 ppb. The increase in O_3 during the daytime occurs at a slower rate of about 2 ppb/h. The NO_x levels at XC are much lower than those at ZZL. The few diurnal variations in NO_x suggest this site is less impacted by direct human influence.

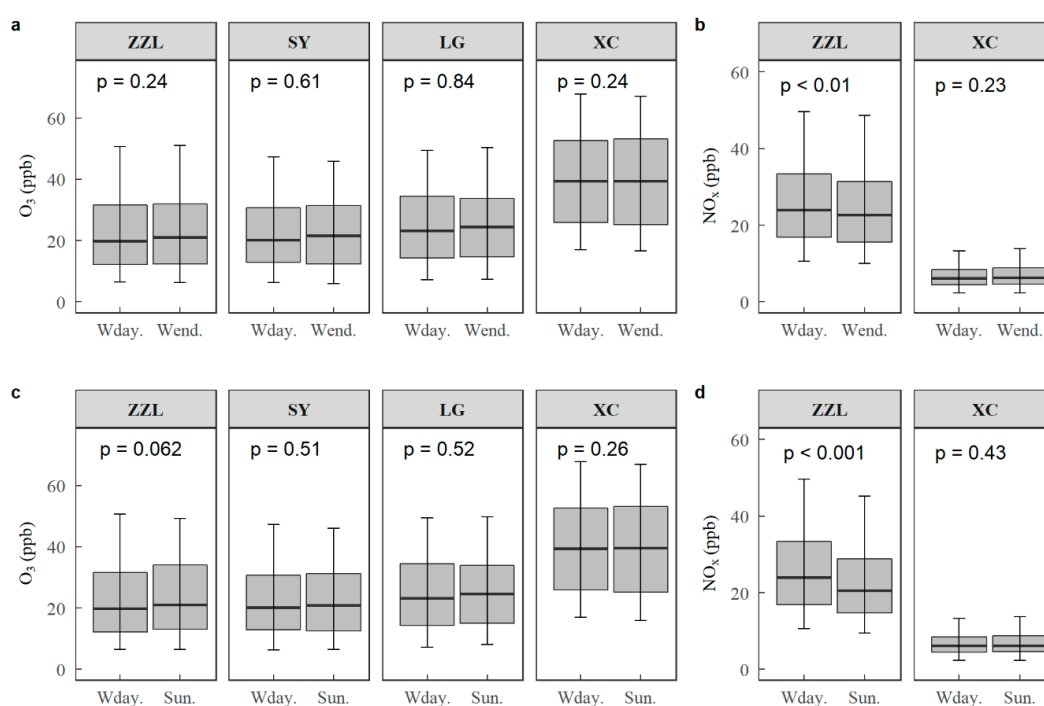


Figure 2. Boxplot of O_3 and NO_x air concentrations at all representative sites from 2011 to 2017. (a) Weekday and weekend O_3 comparison; (b) weekday and weekend NO_x comparison; (c) weekday and Sunday O_3 comparison; and (d) weekday and Sunday NO_x comparison. The horizontal solid lines indicate the median and range, where the top and bottom of the box indicate the 75th and 25th percentiles, respectively. The top and bottom whiskers indicate the 95th and 5th percentiles, respectively. The p -values in figures refer to significance level by Wilcoxon rank–sum test. ZZL is an urban site, LG and SY are suburban sites, and XC is a rural site.

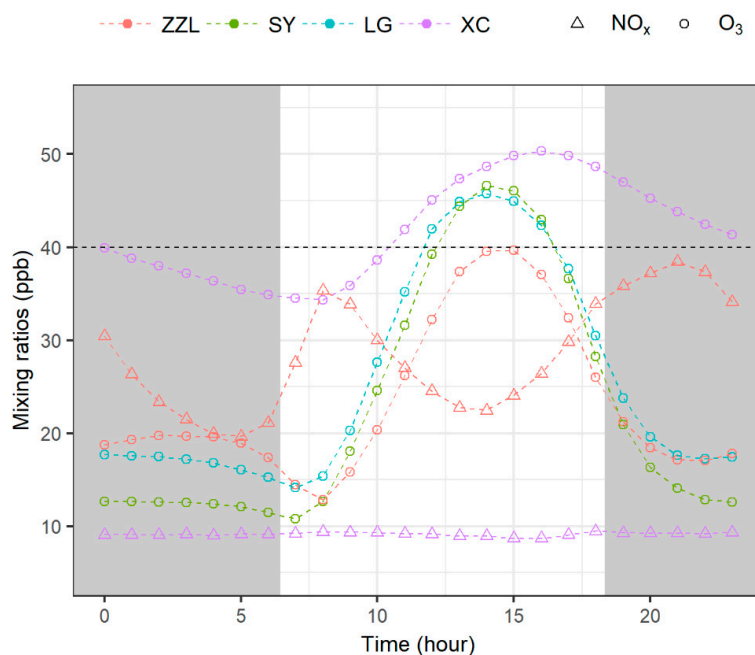


Figure 3. Diurnal variations of hourly mean O_3 and NO_x concentrations at ZZZL, SY, LG, and XC from 2011 to 2017. NO_x data are only valid at ZZZL and XC. The gray horizontal dashed line is the reference of 40 ppb, and the gray area represents nighttime based on local sunrise and sunset averaged throughout the whole year.

3.3. Monthly Variations and the Impacts of Meteorological Factors

The monthly variations of daily maximum 8-h average O_3 and 24-h mean NO_x are shown in Figure 4. Due to the similarity of monthly variations of air pollutants between sites, O_3 and NO_x are only shown at one site. The variations in O_3 are shown at SY to match with meteorological variations at this site. As can be seen from the figure, the monthly O_3 variations show maximum values in the autumn (October) and minimum values in the summer (June) (see Figure 4a). Because XC has very low NO_x levels, monthly NO_x variations are shown at ZZZL. The result shows maximum values in the winter (January) and minimum in the summer (June) (see Figure 4b).

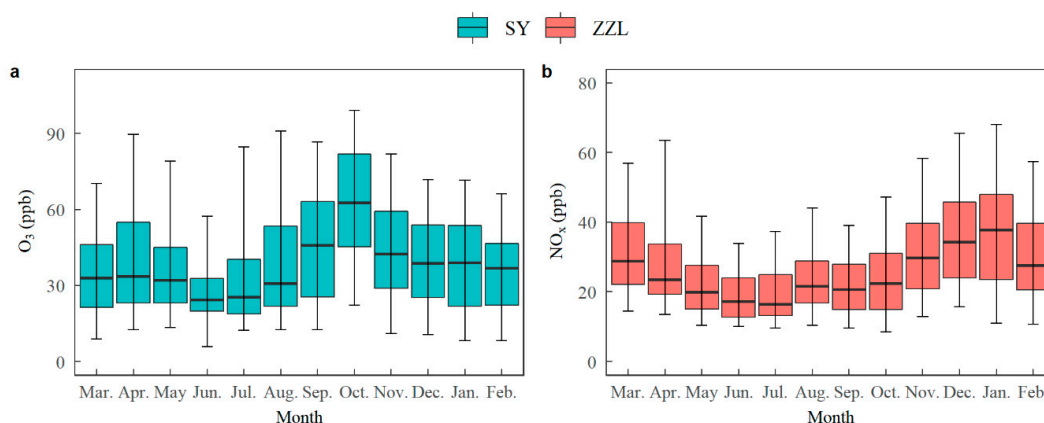


Figure 4. Boxplot of (a) daily maximum 8-h average O_3 , and (b) daily 24-h mean NO_x at the site SY for the 2011 to 2017 period. The horizontal solid lines indicate the median and range, where the top and bottom of the box indicate the 75th and 25th percentiles, respectively. The top and bottom whiskers indicate the 95th and 5th percentiles, respectively.

Monthly variations in meteorological conditions are shown in Figure 5a–f. Wind speed is highest in June and lowest in September (see Figure 5a). Solar radiation is generally higher in the summer

months when the sun is directly overhead in the northern hemisphere (see Figure 5b). Similar to solar radiation, the temperature is also higher in the summer and lower in the winter. The temperature is generally warm in Shenzhen, with median values of daily maximum temperature >20 °C throughout the year (see Figure 5c). The monthly variations in surface pressure show an opposite pattern to the temperature (see Figure 5d). Monthly total precipitation is higher from May to August, which is the main rainy season in Shenzhen (see Figure 5e). The monthly variations in relative humidity are small, with the lowest value in December (see Figure 5f).

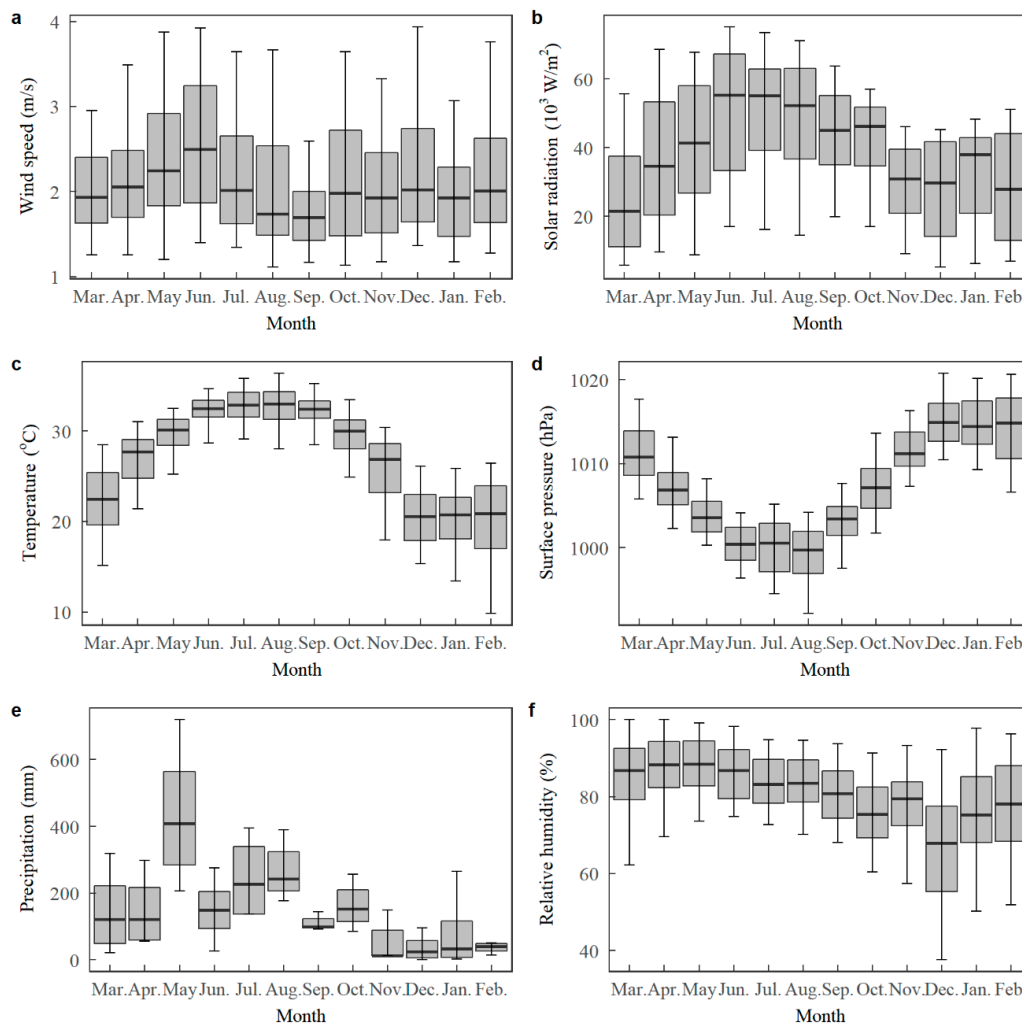


Figure 5. Boxplot of (a) daily total solar radiation (10^3 W/m²), (b) daily mean wind speed (m/s), (c) daily maximum temperature (°C), (d) daily average surface pressure (hPa), (e) monthly total precipitation (mm), and (f) daily average relative humidity (%) at the site SY in each month from 2014 to 2017. The horizontal solid lines indicate the median and range, where the top and bottom of the box indicate the 75th and 25th percentiles, respectively. The top and bottom whiskers indicate the 95th and 5th percentiles, respectively.

The relationships between daily maximum 8-h O₃ and meteorological parameters are shown in Table 4. O₃ is significantly positively correlated with both solar radiation and temperature. The correlation between O₃ and solar radiation is strongest in the winter and moderate in the summer. The correlation between O₃ and temperature is strong in the summer and winter. Wind speed is the least relevant factor, and O₃ and wind speed are negatively correlated only in the winter ($p < 0.001$). O₃ is negatively related to precipitation and relative humidity in all seasons. The relationship between

O₃ and surface pressure is inconsistent in different seasons with a negative relationship in the summer but a positive one in other seasons.

Table 4. Analysis of the relationships between daily maximum 8-h O₃ and meteorological parameters based on Spearman's rank correlation. SR is the daily total solar radiation (W/m²), WS is the average daily wind speed (m/s), T is the daily maximum air temperature (°C), Prep is the daily total precipitation (mm), RH is the average daily relative humidity (%), and SP is the daily average surface pressure (hPa).

Season	SR	WS	T	Prep	RH	SP
Spring	0.35 ***	−0.04	0.11 *	−0.25 ***	−0.51 ***	0.13 *
Summer	0.32 ***	−0.10	0.59 ***	−0.42 ***	−0.48 ***	−0.42 ***
Autumn	0.50 ***	−0.12	0.20 **	−0.38 ***	−0.55 ***	0.13 *
Winter	0.70 ***	−0.28 ***	0.46 ***	−0.58 ***	−0.59 ***	0.18 **
Overall	0.34 ***	−0.17***	0.10 ***	−0.42 ***	−0.57 ***	0.12 ***

The value is marked as bold when the absolute value is greater than 0.3. *, **, and *** represent significance levels of $p < 0.05$, $p < 0.01$, and $p < 0.001$ respectively.

The relationship between high O₃ air concentrations and wind speed/direction are shown in Figure 6. As can be seen from the figure, the high concentrations of O₃ (greater than the 90th percentile for all observations) are controlled by a westerly wind direction with wind speeds of about 2–4 m/s for all seasons. The pattern is most distinct in the summer, with a single source of pollution from the northwest. In the autumn and winter seasons, there is obviously another pollution source from the northeast wind direction. The pattern is distinctive during the wintertime, where the probability of high O₃ levels controlled by the northeast wind direction can reach as high as 0.7 with a wind speed of 6–9 m/s. The conditional probability of high O₃ levels experienced for the southerly-like wind directions is very low in all seasons.

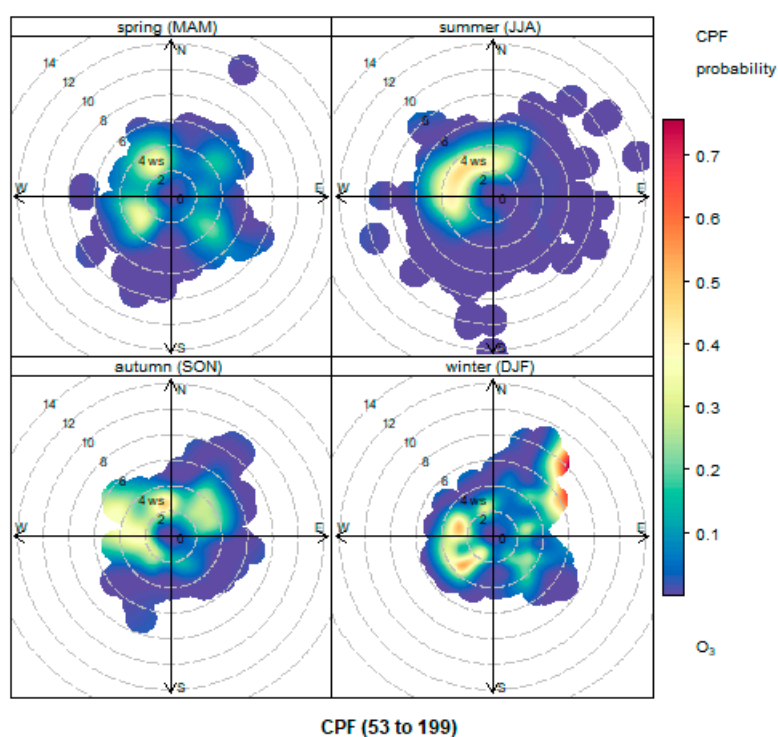


Figure 6. Polar plot of O₃ air concentrations at site SY in each season based on the conditional probability function (CPF) function for the higher percentiles (from 90th = 53 ppb to 100th = 199 ppb).

3.4. Trends of O₃ and NO_x from 2011 to 2017

The percentage of changes per year and the 95% confidence intervals (CIs) of the daily maximum 8-h O₃ and daily 24-h mean NO_x from 2011 to 2017 are shown in Figure 7. The 8-h O₃ shows an increase at all sites (see Figure 7a). The overall O₃ growth rate follows the order of the urbanization rate across all sites (ZZL > SY > LG > XC). The increasing trends at ZZL and SY are significant with an estimated rate of 4.3% (95% CIs: 0.96, 8.25) per year ($p < 0.05$) and 3.61% (95% CIs: 0.36, 7.6) per year ($p < 0.05$), respectively. NO_x decreased significantly at both sites (see Figure 7b). The decreasing rate is faster at ZZL, with an estimated rate of -5.85% (95% CIs: $-7.99, -2.72$) per year ($p < 0.001$), compared with -4.14% (95% CIs: $-6.96, -0.26$) per year at XC ($p < 0.05$).

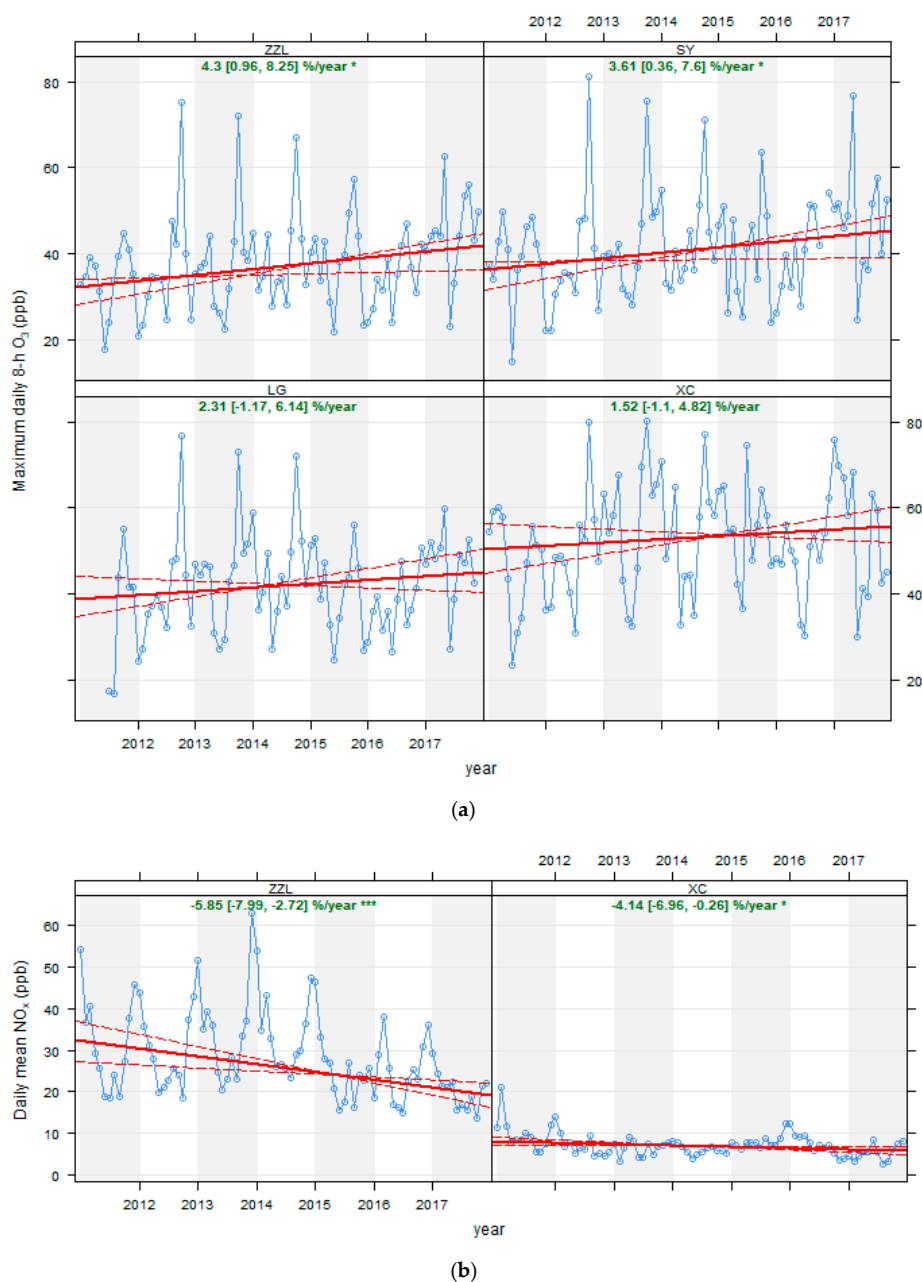


Figure 7. The trend of (a) daily maximum 8-hour average O₃, and (b) daily 24-h mean NO_x from 2011 to 2017. The solid red line shows the trend estimate, and dashed red lines show the 95% confidence intervals for the trend based on resampling methods. The overall trend is shown at the top as the percentage of changes per year and the 95% confidence intervals of the slope. * and *** represent to the significance levels of $p < 0.05$ and $p < 0.001$, respectively.

The Theil-Sen trends of the maximum daily 8-h O_3 and daily 24-h mean NO_x for all representative sites during a specific period from 2011 to 2017 are shown in Table 5. The decline of NO_x is fastest in the winter, with an average decline rate of -7.87% ($p < 0.001$) at the urban site and -9.45% ($p < 0.1$) at the rural site. The increase in O_3 is fastest in the winter at more urbanized sites, with an average growth rate of 6.02% ($p < 0.1$) at the urban site and 8.89% ($p < 0.1$) at the suburban site. A negative trend ($p > 0.1$) is mainly found at less urbanized sites (LG and XC) in the autumn.

Table 5. Theil-Sen trend of daily maximum 8-h average O_3 and 24-h mean NO_x values for all representative sites from 2011 to 2017 (%).

Sites/Variable	ZZL/ O_3	SY/ O_3	LG/ O_3	XC/ O_3	ZZL/ NO_x	XC/ NO_x
Spring	3.55	2.66	4.9	2.42	-5.36^*	-3.51
Summer	6.09	1.77	6.43	4.32	-3.15	-4.77
Autumn	1.36	0.14	-1.94	-1.13	-3.89	2.45
Winter	6.02^+	8.89^+	6.03	3.98	-7.87^{***}	-9.45^+

Values are shown as percentage changes per year. $+$, $*$, and $***$ represent significance levels at $p < 0.1$, $p < 0.05$, and $p < 0.001$, respectively.

The Theil-Sen trends of the daily maximum 1-h O_3 from 2011 to 2017 are shown in Table 6. The overall trends of daily maximum 1-h O_3 are positive at all sites ($p > 0.1$). The overall O_3 growth rate follows the order of the urbanization rate at the urban and suburban sites ($ZZL > SY > LG$). The slight decline in O_3 occurs mainly at less urbanized sites in autumn, i.e., SY, LG, and XC. Only the urban site ZZL increases in all seasons. O_3 increases faster on the weekend than on weekdays at all sites. In particular, the increasing trend of ZZL during the weekend is significant, with an estimated rate of 3.13% (95% CIs: $-0.35, 6.87$) per year ($p < 0.1$).

Table 6. Theil-Sen trends of the daily maximum 1-h O_3 for all representative sites from 2011 to 2017 (%).

Season	ZZL	SY	LG	XC
Spring	1.47 (−2.13, 8.57)	0.93 (−3.91, 11.68)	1.65 (−3.18, 9.33)	0.52 (−2.49, 5.11)
Summer	3.22 (−4.69, 14.23)	0.99 (−4.37, 13.9)	5.86 (−3.79, 24.35)	3.73 (−4.05, 11.49)
Autumn	0.59 (−5.76, 4.66)	-0.75 (−6.44, 2.49)	-1.8 (−6.65, 1.47)	-1.46 (−7.54, 2.87)
Winter	3.65 (−4.27, 11.1)	4.95 (−3.22, 15.65)	-0.47 (−8.58, 10.29)	2.75 (−2.52, 10.19)
Total	2.5 (−0.46, 6.12)	1.49 (−1.18, 4.62)	0.05 (−3.17, 3.45)	0.95 (−1.24, 3.91)

The overall trend is shown as the percentage of changes per year and the 95% confidence intervals.

4. Discussion

The common autumn (October) O_3 maxima and summer (June) O_3 minima at all representative sites are consistent with seasonal characteristics of O_3 air concentrations in subtropical Asia, including western India [43], central and southwestern Taiwan [44,45], the PRD region [17,46], Hong Kong [28], and the South China Sea area [47]. All those areas are geographically close to each other and have similar atmospheric background conditions. Solar radiation, precipitation, and relative humidity are the most significant impact meteorological factors that affect O_3 daily variations. The formation of O_3 is favored by sunlight and high temperature [5,26,27,48]. The strong positive correlation in the winter between O_3 and both of these meteorological factors is likely due to the cold season, which makes them limiting factors for O_3 production. Surface pressure showed the opposite relationship in the summer and other seasons. O_3 production favors high-pressure systems with the subsidence of air [28,47]. This explains the observed positive relationship between O_3 and surface pressure in all other seasons except summer. This negative relationship in the summer was probably controlled by a synoptic-scale feature with the co-product of the negative correlation between temperature and pressure [48]. The negative correlation between O_3 and relative humidity and precipitation explains the summer O_3 trough. With an increase in relative humidity, the cloud abundance usually increases

at the same time, and the photochemical processes of O₃ production will decrease [27]. Rainy weather is also not conducive for O₃ production, and heavy rain will remove O₃ from the air [46].

In contrast, wind speed is the least relevant factor and is only negatively related to O₃ levels in the winter. Higher wind speed will increase the turbulence of the air and cause dispersion of O₃ [28]. The negative relationship between O₃ and wind speed in winter might be influenced by the wind direction in winter which is an important factor that affects O₃ transport [5]. Wind direction is found more important for influencing air pollutant levels. Shenzhen has at least two different sources of air pollution. One is a more regional emission source from the west and is active throughout the year. Emissions from the shipping business on the Pearl River Estuary and industrial activities in Guangzhou and Foshan to the west of Shenzhen might contribute to the continuous regional sources [49]. The high concentrations associated with the northeasterly wind in the winter confirms that the impact of air pollutant transport from northern China [5]. Interestingly, there are no substantial air pollutants associated with the southerly winds in all seasons, which means that contribution of air pollutants from big cities to the south of Shenzhen (i.e., Hong Kong) are less important in impacting air pollutants in Shenzhen.

The difference in NO_x air concentrations is significant between weekdays and the weekend at the urban site. This is probably caused by a weekly routine of human activities. Traffic volume is increased in the city center during workdays. Similar to a previous study result for the PRD region, we also found no statistically significant difference between weekdays and the weekend at all sites in Shenzhen [46]. However, the O₃ weekend effect was significant ($p = 0.062$) at the urban site, with O₃ levels being 1.19 ppb higher on Sunday than on weekdays. O₃ is elevated mainly by less on-road vehicular emissions on the weekend with NO_x reduction and a lowered O₃ titration effect [24,46,50]. In our study, we found the difference in O₃ and NO_x air concentrations between weekday and Saturday were less than those between Saturday and Sunday. A carryover of heavy Friday evening emissions is likely explained the diminished weekday and Saturday O₃ difference [50]. Overtime work on Saturday might also be an important factor. Individual mobility studies show that a Saturday morning peak of passengers is significant, indicating a large proportion of citizens working on that day [51]. Moreover, heavy-duty trucks that contribute to strong emissions of NO_x are more active on Saturday because of fewer traffic restrictions [52].

Different from a previous study that showed that central areas of Shenzhen had higher 1-h and 8-h O₃ [17], we showed results similar to most large cities whereby the urban site has lower O₃ compared with other sites [18,23,26]. The reliability of the previous study is questionable because only one-year observations were used and no statistical comparison was performed. Shenzhen had a lower maximum 1-h, 8-h, and cumulative O₃, as well as exceedances of O₃, compared with suburban and rural sites. The annual mean levels that are lower ($p > 0.05$) at SY than at ZZL may be caused by the low nighttime O₃ at SY, possibly related to continuous emissions of NO_x from industrial activities [53–55]. The characteristics of the O₃ relationship between urban, suburban, and rural sites can be explained by O₃ photochemical sensitivity as indicated by the O₃ diurnal pattern. The sharp decline in O₃ at the urban site in the early morning is mainly caused by the strong titration effect resulting from high levels of NO from traffic emissions when sunlight is limited for O₃ production [53]. The slower O₃ increasing rate at the urban site than at the suburban sites suggests O₃ production might be limited by VOC availability [21,27].

The faster daytime O₃ increasing rates at the suburban sites suggest a more suitable photochemical environment. The highest O₃ daily peak and fastest O₃ production rate at SY were possibly due to the abundance of both precursors. We previously reported high levels of NO₂ in the surrounding area of SY, which were even higher than NO₂ levels at the urban center [55]. Additionally, larger sources of VOCs are from vegetation emissions [21,23,30]. Moreover, industrial and construction activities are also active in suburban areas; both are major sources of anthropogenic VOC emissions [54]. According to research on O₃ at a coastal site in South China, the highest O₃ levels at the rural coastal site are

probably due to weaker NO titration and a high O₃ production rate because of stronger oxidative capacity in the air [56]. VOC data need to be measured as well to understand the O₃ dynamics.

The overall NO_x levels decreased significantly from 2011 to 2017. Winter has the highest NO_x levels and the fastest decline rate. NO_x is high in winter because of more emissions and longer NO_x lifetime during the cold season [26]. In northern China, emissions from coal for heating are substantial; however, as a southern city, Shenzhen does not have central heating in the winter. As can be seen from the pollution rose map, the air pollutant levels in Shenzhen during the wintertime are greatly impacted by prevailing northeast winds which bring polluted air masses from northern China [5,28,47]. The fastest decline in winter at both sites is possibly attributed to the effectiveness of NO_x control in northern China [15].

Different from previous simulation results, both daily maximum 1-h and 8-h O₃ showed overall increases from 2011 to 2017 at all sites [15,25]. There is a clear linkage between the degree of urbanization and the direction of the O₃ trends. The increases in O₃ are profound in the winter at more urbanized sites. This rise can be attributed to increases in O₃ from the transport of continental air masses by northeasterly wind and a lowered O₃ titration effect by NO due to the NO_x reduction [23,57]. A small decline in O₃ occurred mainly at less urbanized sites in the autumn, the highest O₃ season [22]. This implies that the photochemical sensitivity might shift from being VOC-sensitive to NO_x-sensitive in the autumn when photochemical reactions are the most active [19,57]. The increasing changes in 1-h O₃ at all sites indicate that the O₃ sensitivity in the afternoon might not be limited by NO_x availability in Shenzhen [57].

Great challenges remain in controlling O₃ in Shenzhen. Generally speaking, the O₃ chemistry is mainly VOC-sensitive. As NO_x decreases, O₃ levels increase at all sites, with a faster increasing rate at more urbanized areas, posing greater human health risks in areas with high population density. Our results showed a slight decline of O₃ in autumn, which means that controlling NO_x emissions in this period would be the most effective way of lowering the O₃ levels in the less urbanized areas. For the more urbanized sites, emphasis should be placed on VOC reduction. The national VOC reduction strategy is specified in the 13th five-year plan (2015–2020). The goal was set to reduce major industrial VOC emissions by 10% compared with the 2015 level [58]. In Southern China, VOC emissions are dominated by biogenic sources [32]. More work is needed for spatial variability and the O₃ formation potential of VOCs for more efficient O₃ control management.

5. Conclusions

In this study, four stations, including one urban, one rural, and two suburban sites in Shenzhen, were investigated for characteristics and trends of O₃ air pollution from 2011 to 2017. O₃ matched seasonal O₃ characteristics of subtropical Asia, i.e., a maximum in the autumn (October) and a minimum in the summer (June). Solar radiation, precipitation, and relative humidity are the most important meteorological factors that affect O₃ daily variations.

Wind speed is the least relevant factor, but wind direction is important in impacting the presence of high O₃ air concentrations. Shenzhen has at least two different sources of air pollution. One is a more regional emission source from the west and is active throughout the year. Another source is active mainly in the winter, where the high concentrations are associated with the northeasterly wind indicating the impact of air pollutant transport from northern China. The impact of the southerly wind is minimal compared with other wind directions.

O₃ pollution is serious in Shenzhen, with about 28–53% of days per year exceeding the WHO ambient O₃ guideline, and about 1–3 times above the limits for vegetation protection. Both the human population and vegetation are exposed to high O₃, and more exceedances occur at the suburban and rural sites than at the urban site.

The O₃ weekend effect is significant ($p = 0.062$) at the urban site with O₃ levels of 1.19 ppb higher on Sunday than on weekdays. A carryover of heavy Friday evening emissions and overtime work on Saturday might be the primary reason for a diminishing weekday and Saturday O₃ difference.

Both 1-h and 8-h O₃ are increasing at all sites, opposite to the trend of NO_x levels. The rapid decline in NO_x in the winter might be related to the transport of cleaner air masses from northern China. The increase in O₃ is fastest in the winter at more urbanized sites. This can be attributed to the transport of elevated O₃ from northern China and a reduced O₃ titration effect with NO_x reduction. A slight decline in O₃ occurs at less urbanized sites in autumn. This might be caused by photochemical sensitivity shifting from being VOC-sensitive to NO_x-sensitive during this period.

Our results show faster O₃ increases in more urbanized areas, which brings greater human health risks to areas with high population density. Great challenges remain in controlling O₃ in Shenzhen with the reduction of NO_x. VOC reduction should be emphasized in more urbanized areas, while NO_x reduction in the autumn would be the most effective way of controlling O₃ levels. The characteristics and trends of VOCs need to be studied as well to understand O₃ dynamics for more efficient O₃ control.

Author Contributions: Data curation, L.Z. and C.Z.; formal analysis, D.H.; funding acquisition, Q.L. and B.H.; methodology, D.H. and X.W.; project administration, Q.L.; software, G.L.; supervision, Q.L.; visualization, L.S.; writing—original draft, D.H.; writing—review and editing, Q.L. and X.W.

Funding: This study was supported by the Innovation of Science and Technology Commission of Shenzhen Municipality via Grants JCYJ20170413164957461, in part by the Science Technology and Innovation Committee of Shenzhen Municipality under Grant GGF2017073114031767, in part by the Natural Science Foundation of China (NSFC) via Grant 41701167 and U1435215, and in part by Excellent Youth Innovation Fund from Shenzhen Institutes of Advanced Technology via Grant Y5G007.

Conflicts of Interest: The authors declare no conflict of interest.

References

1. Chan, C.K.; Yao, X. Air pollution in mega cities in China. *Atmos. Environ.* **2008**, *42*, 1–42. [CrossRef]
2. Cannistraro, G.; Cannistraro, M.; Cannistraro, A.; Galvagno, A. Analysis of the Air Pollution in the Urban Center of Four Sicilian Cities. *Int. J. Heat Technol.* **2016**, *34*, 219–225. [CrossRef]
3. Cannistraro, M.; Ponterio, L.; Cao, J. Experimental study of air pollution in the urban centre of the city of Messina. *MMC* **2018**, *79*, 133–139. [CrossRef]
4. Matus, K.; Nam, K.M.; Selin, N.E.; Lamsal, L.N.; Reilly, J.M.; Paltsev, S. Health damages from air pollution in China. *Glob. Environ. Chang.* **2012**, *22*, 55–66. [CrossRef]
5. Wang, T.; Xue, L.; Brimblecombe, P.; Lam, Y.F.; Li, L.; Zhang, L. Ozone pollution in China: A review of concentrations, meteorological influences, chemical precursors, and effects. *Sci. Total Environ.* **2017**, *575*, 1582–1596. [CrossRef] [PubMed]
6. Paoletti, E. Impact of ozone on Mediterranean forests: A review. *Environ. Pollut.* **2006**, *144*, 463–474. [CrossRef] [PubMed]
7. Feng, Z.; Hu, E.; Wang, X.; Jiang, L.; Liu, X. Ground-level O₃ pollution and its impacts on food crops in China: A review. *Environ. Pollut.* **2015**, *199*, 42–48. [CrossRef] [PubMed]
8. Sillman, S. The relation between ozone, NO_x and hydrocarbons in urban and polluted rural environments. *Atmos. Environ.* **1999**, *33*, 1821–1845. [CrossRef]
9. Monks, P.S.; Archibald, A.T.; Colette, A.; Cooper, O.; Coyle, M.; Derwent, R.; Fowler, D.; Granier, C.; Law, K.S.; Mills, G.E.; et al. Tropospheric ozone and its precursors from the urban to the global scale from air quality to short-lived climate forcer. *Atmos. Chem. Phys.* **2015**, *15*, 8889–8973. [CrossRef]
10. The State Council of the People's Republic of China. The 12th Five-Year Plan for National Economic and Social Development of the People's Republic of China. Available online: http://www.gov.cn/zhengce/content/2016-12/05/content_5143290.htm (accessed on 9 November 2018). (In Chinese)
11. Gu, D.; Wang, Y.; Smeltzer, C.; Liu, Z. Reduction in NO_x emission trends over China: Regional and seasonal variations. *Environ. Sci. Technol.* **2013**, *47*, 12912–12919. [CrossRef] [PubMed]
12. de Foy, B.; Lu, Z.; Streets, D.G. Satellite NO₂ retrievals suggest China has exceeded its NO_x reduction goals from the twelfth Five-Year Plan. *Sci. Rep.* **2016**, *6*, 35912. [CrossRef] [PubMed]
13. Liu, F.; Zhang, Q.; Zheng, B.; Tong, D.; Yan, L.; Zheng, Y.; He, K. Recent reduction in NO_x emissions over China: Synthesis of satellite observations and emission inventories. *Environ. Res. Lett.* **2016**, *11*, 114002. [CrossRef]

14. Qu, Z.; Henze, D.K.; Capps, S.L.; Wang, Y.; Xu, X.; Wang, J.; Keller, M. Monthly top-down NO_x emissions for China (2005–2012): A hybrid inversion method and trend analysis. *J. Geophys. Res. Atmos.* **2017**, *122*, 4600–4625. [[CrossRef](#)]
15. Wang, S.; Xing, J.; Zhao, B.; Jang, C.; Hao, J. Effectiveness of national air pollution control policies on the air quality in metropolitan areas of China. *J. Environ. Sci.* **2014**, *26*, 13–22. [[CrossRef](#)]
16. Liu, X.; Heilig, G.K.; Chen, J.; Heino, M. Interactions between economic growth and environmental quality in Shenzhen, China's first special economic zone. *Ecol. Econ.* **2007**, *62*, 559–570. [[CrossRef](#)]
17. Wang, L.; Bai, Y.; Zhang, F.; Wang, W.; Liu, X.; Krafft, T. Spatiotemporal Patterns of Ozone and Cardiovascular and Respiratory Disease Mortalities Due to Ozone in Shenzhen. *Sustainability* **2017**, *9*, 559. [[CrossRef](#)]
18. Liu, Y.; Chen, S.; Xu, J.; Liu, X.; Wu, Y.; Zhou, L.; Cheng, J.; Ma, H.; Zheng, J.; Lin, D.; et al. The association between air pollution and outpatient and inpatient visits in Shenzhen, China. *Int. J. Environ. Res. Public Health* **2018**, *15*, 178. [[CrossRef](#)] [[PubMed](#)]
19. Wang, N.; Lyu, X.P.; Deng, X.J.; Guo, H.; Deng, T.; Li, Y.; Wang, S.Q. Assessment of regional air quality resulting from emission control in the Pearl River Delta region, southern China. *Sci. Total Environ.* **2016**, *573*, 1554–1565. [[CrossRef](#)] [[PubMed](#)]
20. Yang, F.; Goldmann, M.; Lagercrantz, J. *Sustainable Mobility the Chinese Way—Opportunities for European Cooperation and Inspiration*; Exakta Print: Malmö, Sweden, 2018; pp. 1–107. ISBN 978-91-87379-45-1.
21. Paoletti, E.; de Marco, A.; Beddows, D.C.S.; Harrison, R.M.; Manning, W.J. Ozone levels in European and USA cities are increasing more than at rural sites, while peak values are decreasing. *Environ. Pollut.* **2014**, *192*, 295–299. [[CrossRef](#)] [[PubMed](#)]
22. Simon, H.; Reff, A.; Wells, B.; Xing, J.; Frank, N. Ozone trends across the United States over a period of decreasing NO_x and VOC emissions. *Environ. Sci. Technol.* **2015**, *49*, 186–195. [[CrossRef](#)] [[PubMed](#)]
23. Sicard, P.; Serra, R.; Rossello, P. Spatiotemporal trends in ground-level ozone concentrations and metrics in France over the time period 1999–2012. *Environ. Res.* **2016**, *149*, 122–144. [[CrossRef](#)] [[PubMed](#)]
24. Li, J.; Lu, K.; Lv, W.; Li, J.; Zhong, L.; Ou, Y.; Chen, D.; Huang, X.; Zhang, Y. Fast increasing of surface ozone concentrations in Pearl River Delta characterized by a regional air quality monitoring network during 2006–2011. *J. Environ. Sci.* **2014**, *26*, 23–36. [[CrossRef](#)]
25. Li, Y.; Lau, A.K.H.; Fung, J.C.H.; Zheng, J.; Liu, S. Importance of NO_x control for peak ozone reduction in the Pearl River Delta region. *J. Geophys. Res. Atmos.* **2013**, *118*, 9428–9443. [[CrossRef](#)]
26. Xie, M.; Zhu, K.; Wang, T.; Chen, P.; Han, Y.; Li, S.; Zhuang, B.; Shu, L. Temporal characterization and regional contribution to O₃ and NO_x at an urban and a suburban site in Nanjing, China. *Sci. Total Environ.* **2016**, *551*, 533–545. [[CrossRef](#)] [[PubMed](#)]
27. Tong, L.; Zhang, H.; Yu, J.; He, M.; Xu, N.; Zhang, J.; Qian, F.; Feng, J.; Xiao, H. Characteristics of surface ozone and nitrogen oxides at urban, suburban and rural sites in Ningbo, China. *Atmos. Res.* **2017**, *187*, 57–68. [[CrossRef](#)]
28. Wang, T.; Wu, Y.Y.; Cheung, T.F.; Lam, K.S. A study of surface ozone and the relation to complex wind flow in Hong Kong. *Atmos. Environ.* **2001**, *35*, 3203–3215. [[CrossRef](#)]
29. Zhang, H.; Wang, Y.; Hu, J.; Ying, Q.; Hu, X.-M. Relationships between meteorological parameters and criteria air pollutants in three megacities in China. *Environ. Res.* **2015**, *140*, 242–254. [[CrossRef](#)] [[PubMed](#)]
30. Chameides, W.L.; Lindsay, R.W.; Richardson, J.; Kiang, C.S. The role of biogenic hydrocarbons in urban photochemical smog: Atlanta as a case study. *Science* **1988**, *241*, 1473–1475. [[CrossRef](#)] [[PubMed](#)]
31. Kleinman, L.I.; Daum, P.H.; Imre, D.; Lee, Y.N.; Nunnermacker, L.J.; Springston, S.R.; Weinstein-Lloyd, J.; Rudolph, J. Ozone production rate and hydrocarbon reactivity in 5 urban areas: A cause of high ozone concentration in Houston. *Geophys. Res. Lett.* **2002**, *29*. [[CrossRef](#)]
32. Jin, X.; Holloway, T. Spatial and temporal variability of ozone sensitivity over China observed from the Ozone Monitoring Instrument. *J. Geophys. Res. Atmos.* **2015**, *120*, 7229–7246. [[CrossRef](#)]
33. Shenzhen Statistics Bureau, NBS Survey Office in Shenzhen. Shenzhen Statistical Yearbook—2017. Available online: <http://www.szsj.gov.cn/xxgk/zfxgkml/tjsj/tjnj/> (accessed on 1 November 2018). (In Chinese)
34. China Meteorological Administration. *China Atmospheric Composition Monitoring Service Specification*; China Meteorological Press: Beijing, China, 2012; pp. 1–112. (In Chinese)
35. Song, Y.; Linderholm, H.; Chen, D.; Walther, A. Trends of the thermal growing season in China, 1951–2007. *Int. J. Climatol.* **2010**, *30*, 33–43. [[CrossRef](#)]
36. Spearman, C. The proof and measurement of association between two things. *Am. J. Psychol.* **1904**, *15*, 72–101. [[CrossRef](#)]

37. Wilcoxon, F. Individual comparisons by ranking methods. *Biom. Bull.* **1945**, *1*, 80–83. [[CrossRef](#)]
38. Carslaw, D.C.; Ropkins, K. Openair—An R package for air quality data analysis. *Environ. Model. Softw.* **2012**, *27–28*, 52–61. [[CrossRef](#)]
39. Sen, P.K. Estimates of the regression coefficient based on Kendall's tau. *J. Am. Stat. Assoc.* **1968**, *63*, 1379–1389. [[CrossRef](#)]
40. R Core Team. *R: A Language and Environment for Statistical Computing*; R Foundation for statistical computing: Vienna, Austria, 2018; Available online: <https://www.R-project.org/> (accessed on 29 November 2018).
41. Wickham, H. *ggplot2: Elegant Graphics for Data Analysis*; Springer: New York, NY, USA, 2016.
42. World Health Organization. Air Quality Guidelines for Particulate Matter, Ozone, Nitrogen Oxide and Sulfur Dioxide—Global Update. 2005. Available online: http://www.who.int/phe/health_topics/outdoorair/outdoorair_aqg/en/ (accessed on 9 November 2018).
43. Lal, S.; Naja, M.; Subbaraya, B.H. Seasonal variations in surface ozone and its precursors over an urban site in India. *Atmos. Environ.* **2000**, *34*, 2713–2724. [[CrossRef](#)]
44. Lin, C.Y.; Wang, Z.; Chou, C.C.K.; Chang, C.C.; Liu, S.C. A numerical study of an autumn high ozone episode over southwestern Taiwan. *Atmos. Environ.* **2007**, *41*, 3684–3701. [[CrossRef](#)]
45. Tsai, D.H.; Wang, J.L.; Wang, C.H.; Chan, C.C. A study of ground-level ozone pollution, ozone precursors and subtropical meteorological conditions in central Taiwan. *J. Environ. Monit.* **2008**, *10*, 109–118. [[CrossRef](#)] [[PubMed](#)]
46. Zheng, J.; Zhong, L.; Wang, T.; Louie, P.K.K.; Li, Z. Ground-level ozone in the Pearl River Delta region: Analysis of data from a recently established regional air quality monitoring network. *Atmos. Environ.* **2010**, *44*, 814–823. [[CrossRef](#)]
47. Wang, T.; Guo, H.; Blake, D.R.; Kwok, Y.H.; Simpson, I.J.; Li, Y.S. Measurements of trace gases in the inflow of South China Sea background air and outflow of regional pollution at Tai O, southern China. *J. Atmos. Chem.* **2005**, *52*, 295–317. [[CrossRef](#)]
48. Shan, W.; Yin, Y.; Zhang, J.; Ji, X.; Deng, X. Surface ozone and meteorological condition in a single year at an urban site in central–eastern China. *Environ. Monit. Assess.* **2009**, *151*, 127–141. [[CrossRef](#)] [[PubMed](#)]
49. Tao, J.; Shen, Z.; Zhu, C.; Yue, J.; Cao, J.; Liu, S.; Zhu, L.; Zhang, R. Seasonal variations and chemical characteristics of sub-micrometer particles (PM1) in Guangzhou, China. *Sci. Total Environ.* **2012**, *118*, 222–231. [[CrossRef](#)]
50. Blanchard, C.L.; Tanenbaum, S.J. Differences between weekday and weekend air pollutant levels in southern California. *J. Air Waste Manag. Assoc.* **2003**, *53*, 816–828. [[CrossRef](#)] [[PubMed](#)]
51. Liu, L.; Hou, A.; Biderman, A.; Ratti, C.; Chen, J. Understanding individual and collective mobility patterns from smart card records: A case study in Shenzhen. In Proceedings of the 12th International IEEE Conference on Intelligent Transportation Systems, St Louis, MO, USA, 4–7 October 2009.
52. Yu, X.; Yuan, Z.; Fung, J.C.H.; Xue, J.; Li, Y.; Zheng, J.; Lau, A.K.H. Ozone changes in response to the heavy-duty diesel truck control in the Pearl River Delta. *Atmos. Environ.* **2014**, *88*, 269–274. [[CrossRef](#)]
53. Zhang, R.Y.; Lei, W.F.; Tie, X.X.; Hess, P. Industrial emissions cause extreme urban ozone diurnal variability. *Proc. Natl. Acad. Sci. USA* **2004**, *101*, 6346–6350. [[CrossRef](#)] [[PubMed](#)]
54. Zacharias, J.; Ma, B. Industrial zone development policy related to real estate and transport outcomes in Shenzhen, China. *Land Use Policy* **2015**, *47*, 382–393. [[CrossRef](#)]
55. Huang, D.; Li, Q.; Li, G.; Wang, X.; Sun, L. Tougher Targets for China's Clean Air Cities? Implications from Air Quality Assessment in Shenzhen. *Preprints* **2018**, 2018100101. [[CrossRef](#)]
56. Wang, H.; Lyu, X.; Guo, H.; Wang, Y.; Zou, S.; Ling, Z.; Wang, X.; Jiang, F.; Zeren, Y.; Pan, W.; et al. Ozone pollution around a coastal region of South China Sea: Interaction between marine and continental air. *Atmos. Chem. Phys.* **2018**, *18*, 4277–4295. [[CrossRef](#)]
57. Wang, X.; Zhang, Y.; Hu, Y.; Zhou, W.; Zeng, L.; Hu, M.; Cohan, D.; Russell, A. Decoupled direct sensitivity analysis of regional ozone pollution over the Pearl River Delta during the PRIDE-PRD2004 campaign. *Atmos. Environ.* **2011**, *45*, 4941–4949. [[CrossRef](#)]
58. The State Council of the People's Republic of China. The 13th Five-Year Plan for National Economic and Social Development of the People's Republic of China. Available online: http://www.gov.cn/xinwen/2016-03/17/content_5054992.htm (accessed on 9 November 2018). (In Chinese)

